NACA RM L56F11a

NACA

RESEARCH MEMORANDUM

AERODYNAMIC HEATING OF A WING AS DETERMINED FROM A FREE-FLIGHT ROCKET-MODEL TEST TO MACH NUMBER 3.64

By Andrew G. Swanson and Charles B. Rumsey

Langley Aeronautical Laboratory
Langley Field, Va.

NATIONAL ADVISORY COMMITTEE
FOR AERONAUTICS

WASHINGTON

September 11, 1956
Declassified September 1, 1959

NACA RM L56F11a

NATIONAL ADVISORY COMMITTEE FOR AERONAUTICS

RESEARCH MEMORANDUM

AERODYNAMIC HEATING OF A WING AS DETERMINED FROM A FREE-FLIGHT ROCKET-MODEL TEST TO MACH NUMBER 3.64

By Andrew G. Swanson and Charles B. Rumsey

SUMMARY

As part of a general program to study aerodynamic heating, a wing of aspect ratio 2.9 having a 30° swept leading edge, an unswept trailing edge, and a hexagonal airfoil section was flight tested on a rocket-propelled model to a Mach number of 3.64 and a Reynolds number of 31.9×10^6 (based on wing mean aerodynamic chord of 1.52 feet).

The highest temperatures and heat-transfer rates occurred at the stagnation line on the leading edge of the wing; however, the temperature measurement technique was inadequate for correlating the data with theory. Stanton numbers reduced from the temperature time histories measured at locations other than the stagnation point were in fair agreement with the theoretical results of Van Driest for flat plates with turbulent boundary layers. The use of the Van Driest theory in predicting temperature time histories was shown to give results of good engineering accuracy for the conditions of this test. Under the transient heating conditions of the test, large temperature gradients were found to exist over the surface of the wing. Also, a temperature differential through the skin was measured.

INTRODUCTION

A fairly extensive literature exists on experimental investigations of supersonic aerodynamic heat transfer to bodies of revolution (including various nose shapes) and flat plates, but the data for other components of airplanes and missiles are relatively meager. Preliminary data on heat transfer to such components as wings, canopies, and control surfaces are given in reference 1 for a few values of Mach number and Reynolds number. Details of one of the investigations of reference 1 are available in reference 2 for a 60° delta wing at a Mach number of 1.98. Heat-transfer data for two-dimensional wings, at fairly low Reynolds numbers, are given in reference 3 for Mach numbers in the range 1.5 to 2.0.

As part of a general program by the Langley Pilotless Aircraft Research Division to determine supersonic aerodynamic heat transfer to components, temperature measurements were obtained on a wing mounted as

one of the stabilizing fins mounted on a rocket motor used to propel a conical-nose model. The main objective of the test was to obtain heat-transfer data for the cone. The primary purpose of the wing instrumentation was to obtain data for use in design of NACA research missiles; however, it is believed that the wing is representative of typical supersonic designs and that the data will be of general use and interest. Only the wing data are reported herein.

The wing, of aspect ratio 2.9, had a 30° swept leading edge and an unswept trailing edge and employed a hexagonal airfoil section. The rocket motor propelled the test vehicle to a Mach number of 3.64 and a corresponding free-stream Reynolds number of 31.9×10^6 based on wing mean aerodynamic chord of 1.52 feet. The data are compared with results predicted from the theory of Van Driest for a flat plate with a turbulent boundary layer. The flight test was conducted at the Pilotless Aircraft Research Station at Wallops Island, Va.

SYMBOLS

N_{St} Stanton number, $\frac{h}{(c_p \rho V)_l}$

C_f local skin-friction coefficient

c_p specific heat, $\frac{\text{Btu}}{(\text{slug})(^\circ\text{R})}$

ρ density, slugs/cu ft

ϵ emissivity

σ Stefan-Boltzmann constant, $0.4806 \times 10^{-12} \frac{\text{Btu}}{(\text{sq ft})(\text{sec})(^\circ\text{R})^4}$

t thickness, ft

T temperature, °R

τ time, seconds

V velocity, ft/sec

η_r recovery factor, $\frac{T_{aw} - T_l}{T_t - T_l}$

μ	viscosity, slugs/ft-sec
k	thermal conductivity, $\frac{(\text{Btu})(\text{ft})}{(\text{sq ft})(\text{sec})(^{\circ}\text{R})}$
p	static pressure, lb/sq ft
q	dynamic pressure, lb/sq ft
R	Reynolds number, $\rho Vx/\mu$
x	distance from wing leading edge (measured in free-stream direction), ft
N_{Pr}	Prandtl number, $c_p\mu/k$
c	chord, ft
M	Mach number
h	local aerodynamic heat-transfer coefficient, $\frac{\text{Btu}}{(\text{sec})(\text{sq ft})(^{\circ}\text{R})}$
y	distance along wing surface (measured in direction of conductive heat flow), ft

Subscripts:

l	just outside boundary layer
aw	adiabatic wall
t	stagnation
w	wall (skin)
∞	free stream

MODEL AND INSTRUMENTATION

The general arrangement and pertinent dimensions of the test vehicle are shown in the sketch of figure 1 and in the photograph of figure 2. A detailed sketch of the wing alone is shown in figure 3 with geometric characteristics being given in table I.

The wing was mounted as one of four similar stabilizing fins of the rocket motor (M-5 JATO or Nike missile booster) which was used to propel a conical nose. (See fig. 2.)

Magnesium sheet of 3/16-inch thickness was used for the flat section of the wing and 1/8-inch-thick sheet was used for the leading- and trailing-edge wedge sections. Magnesium spars were welded to the skin at the break lines and ran from root to tip. The leading-edge skin was supported by 3/32-inch-thick magnesium ribs. A weld bead, rounded to approximately semicircular shape, joined the top and bottom skins at both the leading and trailing edges. The wing root was welded along the flat section to a cast magnesium shroud wrapped around the rocket motor nozzle. The tip was sealed with a magnesium plate. The skin surfaces were fairly smooth but were not polished.

The maximum camber, bow (spanwise), and twist of the wing were less than 0.04, 0.20 inch, and 0.3°, respectively. The alinement of the wing with the rocket motor and cone center line was within 1°.

The locations of the iron-constantan thermocouples are given in figure 3 and table II. The thermocouples were all mounted sufficiently far from the ribs for the heat flow into the ribs to have negligible influence on the skin temperatures at the measurement points. The spars may have had some influence on the data obtained after the peak temperature was reached, as is discussed later. Thermocouples 11 and 12 were mounted close to the root to determine heat-sink effects of the fin mounting shroud on fin temperatures. With the exception of thermocouples 3 and 5, all thermocouples were located at the inside surfaces of the skin. Thermocouple 3 measured a temperature on the outside surface, as shown in figure 3, by having the bead (the fused junction of the wires) welded in a hole countersunk about 1/16 inch deep in the outer surface. The diameter of the hole under the bead, through which the wires were led, was about 1/16 inch in diameter. The thermocouple leads were insulated from one another and the skin up to the juncture of the bead. Thermocouple 5 was mounted in a similar fashion at the outer surface of the leading edge at the stagnation point.

Measurements of the temperatures were transmitted to the ground by a telemeter located in the nose cone. The maximum probable error in the temperature measured on the flat portion and the trailing-edge wedge of the wing is $\pm 10^{\circ}$ R. This value is based on a maximum probable error of ± 2 percent of the calibrated full-scale range which is the usual accuracy of Pilotless Aircraft Research Division flight-model instrumentation. However, since the thermocouple telemetric technique includes an in-flight calibration (transmission of three known voltages in addition to the thermocouple readings), the accuracy of these temperatures probably approaches $\pm 5^{\circ}$ R (± 1 percent of full-scale range). Because the temperatures on the leading-edge wedge section exceeded the nominal calibrated

full-scale-range upper limit of 1,020° R by varying amounts, the accuracy of these measurements is less at the maximum values and is probably about ±15° R at 1,100° R.

A more complete discussion of the general methods of thermocouple installation and of the temperature telemetric techniques employed by the Langley Pilotless Aircraft Research Division is presented in reference 4.

TEST AND ANALYSIS

The model was ground launched at an elevation angle of 75°. Temperature data were recorded during and after the burning of the M-5 JATO rocket motor. Velocity data were obtained from a CW Doppler radar, model space position was obtained from an NACA modified SCR 584 tracking radar, and atmospheric data were obtained from a rawinsonde (a radar-tracked sounding balloon). Velocity data were corrected for the wind velocity determined by the rawinsonde.

The temperature time-history data were reduced to Stanton number from the following relation (which is discussed in more detail in refs. 4 and 5:

$$N_{St}\left(c_p\rho V\right)_l = \frac{\left(c_p\rho t\right)_w}{\left(T_{aw} - T_w\right)}\frac{dT_w}{d\tau} + \frac{\sigma\epsilon T_w^4}{\left(T_{aw} - T_w\right)} + \frac{(kt)_w}{\left(T_{aw} - T_w\right)}\frac{\partial^2 T_w}{\partial y^2} \qquad (1)$$

where

$$T_{aw} = T_l + \eta_r\left(T_t - T_l\right) \qquad (2)$$

The data were reduced using a constant recovery factor of 0.89, which is an average value of $\left(N_{Pr}\right)^{1/3}$ (the theoretical recovery factor for a turbulent boundary layer) for the range of wall temperatures of the test.

To determine local flow conditions over the surface of the wing, pressure coefficients were determined from linear theory (ref. 6). Local Mach numbers and static pressures were computed from these coefficients (which are shown in fig. 4) by assuming the total pressure over the wing to be that behind a normal shock using the component of free-stream Mach number normal to the leading edge. Since the stagnation temperature at any Mach number is constant throughout the flow, the local static

temperatures could be computed from the local Mach numbers with the supersonic flow tables. These local temperatures were combined with the pressures to obtain the local densities.

Since the range of local static temperatures was not large, c_{p_l} (local specific heat of air) was assumed to have a constant value of $7.73 \frac{\text{Btu}}{(\text{slug})(^\circ\text{R})}$. This assumption results in negligible error in the N_{St} data presented. The values of specific heat for magnesium as a function of temperature were obtained from reference 7.

Estimates of the radiation term (second term on right-hand side of eq. (1)) showed its effects to be negligible so it was not included in the data reduction. No exact computations of the conduction term (last term of eq. (1)) could be made since there were insufficient temperatures recorded to determine the values of $\partial^2 T_w / \partial y^2$ and, therefore, no conduction effects were included in the data reduction. Approximate calculations did indicate, however, that for about the first 5 to 8 seconds of the flight conduction would have very small effect on the temperature and heat-transfer data (except for those stations near the root). One or two seconds beyond peak temperatures (i.e., after about 10 to 12 sec), the errors introduced in the heat-transfer data, due to neglecting the conduction terms, are no longer negligible but are small and of the same magnitude as the possible errors in the other quantities involved in the data reduction.

At times near peak temperature, the slopes $dT_w/d\tau$ are close to zero, and small differences between relatively large quantities, T_{aw} and T_w, are involved in the data reduction. Consequently, any small errors in those quantities are considerably magnified, which results in large scatter and very poor accuracy. Therefore, values of N_{St} were not calculated in the time range near peak temperatures. For this test the same difficulties exist, to a lesser extent, as the skin begins to heat (i.e., up to about 2 or 3 sec) and, also, when the skin is cooling (i.e., after about 11 sec). For these times the maximum probable error in the N_{St} data is computed to be in the range of ±15 to ±25 percent. When the heating rates are high (i.e., from about 3 to 8 sec), the maximum probable error is computed to be about ±10 percent. The method used in computing the accuracy of the N_{St} data is presented in reference 5 which discusses in some detail the accuracy of the general method used to obtain N_{St} data with rocket-propelled models in the Langley Pilotless Aircraft Research Division.

In the time region near peak temperature, the aerodynamic heat transfer to the skin is approximately the same numerical value as the conductive heat transfer along the skin to the spars. Since conduction was not accounted for in the computation of experimental values of N_{St}, the net result of those conduction effects is to extend the time interval, mentioned previously, over which N_{St} data cannot be obtained.

Experimental recovery factors could not be determined since conduction would also influence these data. It is believed that, if conduction could accurately be accounted for, the experimental recovery factor would not differ greatly from 0.89.

For comparison with the experimental data, theoretical values of Stanton number, based on the local flow conditions of the test, were obtained from the theory of Van Driest for flat plates having turbulent boundary layers (ref. 8). The expression for C_f as given by this reference was modified by use of the Von Kármán similarity law for mixing length as suggested on page 16 of reference 9. The value of N_{St} was taken to be $0.6C_f$ as suggested in reference 10. Local Reynolds numbers were calculated considering the effective length to be the distance from the leading edge.

Theoretical temperature time histories were computed for some of the stations. The Stanton numbers for these calculations were obtained from the Van Driest theory as previously. Skin temperatures were calculated by a step-by-step procedure from equation (1) (with the proper rearrangement of terms). In computing T_{aw}, a constant recovery factor of 0.89 was assumed. Radiation effects were estimated as negligible and conduction was assumed to be zero. For the subsonic portion of the flight, local flow conditions were assumed equal to free-stream conditions. This assumption introduced negligible error since the heat transfer and temperature rise were quite low during this portion of the flight. Supersonic local flow conditions used were those obtained for the reduction of the N_{St} data.

Efforts were made to calculate the temperature at the leading edge (station 5) by using the theory of reference 11. Since a complete time history for station 5 was not available (readings from thermocouple 5 exceeded the calibrated range between 3.3 and 8.8 sec), only a partial analysis could be made.

RESULTS

General

The values of free-stream Mach number, Reynolds number per foot, and stagnation temperature obtained during the flight test are presented as functions of time in figure 5.

Temperature time histories are presented in figures 6 to 9. With minor exceptions, which are discussed later, the general trend is as would be anticipated. The temperatures rose most steeply as the model accelerated and less steeply after rocket motor burn out (about 3.2 sec) until a maximum was reached when the wall temperatures equaled the adiabatic wall temperature. The wall temperature then decreased as the heat stored in the skin was transferred to the cooler boundary layer. The highest temperatures and heat-transfer rates were at the stagnation point (station 5). (The data for station 5 exceeded the calibrated range during the time from 3.3 to 8.8 sec.) Heating rates generally decreased as distance from the leading edge and therefore boundary-layer thickness increased. When the temperature data of figure 6 are considered, it should be noted that the true magnitude of the reductions in heat transfer due to the changes in local flow conditions over the surface of the wing is masked by the increased heat capacity of the thick skin of the wing center section over the thinner skin of the leading and trailing edges.

The data are shown reduced to Stanton number N_{St} in figures 10 to 12. Although there is some scatter in the experimental data, the general trend is in fair agreement with the theory of Van Driest for flat plates with turbulent boundary layers (refs. 8 and 9). Also, the trends of the experimental results are generally compatible when comparisons are made between the data for the various stations. It is believed that accurately accounting for conduction would generally increase the agreement between theory and experiment.

Forward Wedge Section

Analysis proceeds more readily if the temperature and Stanton number data for the forward wedge section are considered together. It is apparent from the temperature time histories of figures 6 and 7 and the N_{St} data of figure 10 that the flow at station 6 was transitional to approximately the time of peak temperature. This transitional flow caused the temperature at station 6 to lag behind the temperature at station 7 even though station 7 was the more rearward one and would normally be expected to be cooler because of increased boundary-layer thickness. Shortly before peak temperature was reached, the transition point must have been only

slightly ahead of station 6 which resulted in a short effective length of turbulent flow and, therefore, in higher heat transfer at station 6 than would have existed if the flow had been turbulent from the leading edge.

The level of the data for station 7 (figs. 7 and 10) indicates predominantly turbulent flow for some distance ahead of station 7. The somewhat low level of the experimental N_{St} data up to 3 seconds (see fig. 10) could be an indication of transitional flow at station 7 but is more apt to be due to scatter in the data.

After the time of peak temperature, the N_{St} data for both stations 6 and 7 (fig. 10) are somewhat above the turbulent theory based on length from the leading edge. The agreement is improved, especially for station 6, if the boundary-layer transition is assumed to occur about halfway from the leading edge to station 6 and the theory is based on length from the transition point. Theoretical values for stations 6 and 7 based on this assumption are also shown in figure 10. Although the agreement is not as good at station 7 as at station 6, the assumption may nevertheless be valid since the data for station 7 would be expected to show greater influence of conduction than the data for station 6. The anomalies due to transition are, of course, incidental to the major premise of reasonably good agreement between the experimental values of N_{St} and those predicted from the Van Driest theory.

If the flow had been turbulent from the leading edge, the temperatures at station 1 (see fig. 7) according to theory should have been somewhat lower than those measured. A short length of laminar flow, extending about one-third of the distance from the leading edge to station 1 (i.e., a length of laminar boundary layer similar to that assumed in regard to stations 6 and 7), would raise the theoretical heating rate sufficiently to result in theoretical temperatures at station 1 equal to those measured.

Flat Section

The data for the stations on the flat section of the wing, figures 8 and 11 show generally the trend that would be expected. Since linear theory predicts practically identical flow conditions over the entire flat section of the wing, heat-transfer rates at a given time would be determined primarily by length from the leading edge, that is, Reynolds number, other things being equal. A measure of inequality is introduced, however, by the proximity of stations 11 and 12 to the large relatively cool mass of the fin mounting shroud. As was anticipated, this heat sink reduced the apparent aerodynamic heat-transfer rates for these stations during the time the skin was heating and increased the rates during the time the skin was cooling by absorbing heat from the skin. Since the conduction effects during the first few seconds were estimated to be only

about 10 percent for even the case of zero temperature rise on the shroud, it is probable that all of the experimental N_{St} data for station 11 are somewhat reduced owing to a thick boundary layer at the wing-body juncture.

The trends of the experimental data for stations 8 and 9 and the good agreement between theory and experiment for these two stations indicate that, after the transitional flow at the leading edge, the heat transfer along this chord line was primarily a function of the usually considered parameters of Reynolds number, Mach number, and T_w/T_l.

From the temperature data of figure 8 and the N_{St} data of figure 11, it would appear that the heat transfer at station 2 was slightly low. The differences between the data obtained and theory are fairly small and are within the range of possible error in the data; however, this small difference (particularly up to 4 sec) may explain some effects noted subsequently. Since the conduction effects for stations 2 and 8 would be expected to be similar, the levels of the N_{St} data for these two stations would tend to substantiate the belief that, for the data presented after peak temperature (12 to 15 sec), the error due to neglecting conduction is about the same value as the remaining possible errors.

Trailing-Edge Wedge Section

As would be expected, the temperature data for stations 4 and 10 on the trailing-edge wedge section (plotted in fig. 9) are quite similar. The data for station 10 are shown reduced to Stanton number in figure 12 and are in fair agreement with the Van Driest theory. In view of the similarity between temperature time histories and local flow conditions for stations 10 and 4, the heat-transfer data for the two stations would also be similar.

Calculated and Measured Temperature Comparison

Although there is some disagreement between the experimental Stanton number data and the values obtained from the theory of Van Driest, the use of the theory in predicting temperatures would give good results for the conditions of this test as is illustrated by the data of figure 13 which compare temperatures calculated by using the theory with the measured temperatures at three stations on one chord line at the 42-percent-span station. The comparison is generally quite good and indicates that for surfaces such as thin wings, which do not deviate too far from a flat plate, the theory will predict temperature time histories with good engineering accuracy, at least for the conditions encountered in this test.

To illustrate more clearly the effects of the leading- and trailing-edge wedge sections on the temperature distribution, a temperature time history for station 9, which is on the flat section of the wing, is presented in figure 13 for a 1/8-inch thickness (the thickness of the skin on the wedge sections) in addition to a time history for the actual skin thickness at station 9 of 3/16 inch. Discounting Reynolds number effects, which would be relatively small, the changes in local flow conditions after each change in slope of the airfoil are seen to have about equal influence on the heat transfer. Also, the increased heat capacity of the thicker skin can be seen to have an effect equal to that of the expansion in reducing the maximum temperature, clearly illustrating that, for rapid transient heating, structural characteristics and aerodynamic phenomona can be equally powerful influences on the temperature distribution.

For this test, changes in N_{St} of ±20 percent of the values of N_{St} computed from Van Driest theory resulted in a variation of about ±10 percent in the maximum temperature rise computed in the temperature time history. The amount of variation in peak temperature for a given variation in N_{St} is, of course, a function of $|T_{aw} - T_w|$ and therefore a function of the particular vehicle, and its trajectory, for which the computations are made.

In computing the temperature histories, a variation of ±20 percent in the static-pressure coefficients resulted in less than 5-percent change in the product ρV. (Variations in the term ρV have, of course, the same effect on temperature time-history calculations as do similar variations in N_{St}.) The ρV product was sensitive, however, to the assumed value of total pressure over the wing surface. A change from an attached oblique shock to a detached normal shock at the wing leading edge resulted in changes of about 10 percent to 50 percent in the values of ρV.

It should be remarked that although the use of the Van Driest turbulent theory should, in most instances, give good engineering accuracy in predicting temperatures over the wing surface, a transition from laminar to turbulent flow could result in actual temperatures near the transition point somewhat higher than those calculated assuming turbulent flow over the entire surface.

In the case of the leading-edge temperature at the stagnation line, a rigorous comparison between experiment and theory could not be made since a complete time history of leading-edge temperature was not obtained (readings from thermocouple 5 exceeded the calibrated range from about 3.3 to 8.8 sec). However, computations of temperature at the stagnation line were made by using heat-transfer coefficients obtained from the theory of reference 11. The values of h were based on the nominal leading-edge diameter of 1/4 inch. The effective thickness was assumed to be 1/8 inch

and the adiabatic wall temperature was assumed as T_t (or recovery factor $\eta_r = 1.0$). As can be seen in figure 14, the temperature history thus computed is in fair agreement with the experimental data available during the heating portion of the flight but is in poorer agreement as to the level and trend during the time the leading edge is cooling. It is believed that the peak temperature predicted is probably representative of the actual temperature of the wing leading edge.

Temperature Gradient Through Skin

An attempt was made to measure the temperature differential through the skin by installing thermocouples at the outside and inside surfaces, stations 3 and 2, respectively. The results are shown in figure 15 together with a differential predicted from reference 12 by assuming a variation of temperature at station 3 proportional to time squared (with axis at $t = 1.0$) and then computing the resulting temperature at the inside surface. The theory gives a temperature differential considerably less than that measured. The methods of reference 13, in which the heat input rather than the variation of temperature on the outside surface is used, gave similar results. Since the thermal properties of the wall do not vary much over the range of temperatures involved, the theoretical results should be fairly exact and it is most probable that the experimental data do not give a true indication of the gradient through the skin since the techniques of measurement were not sufficiently sophisticated to determine accurately the temperature difference through a solid homogeneous wall. The type of thermocouple installation at station 3 (see fig. 3) would tend to create a local hot spot, owing to the decreased mass beneath the thermocouple, which would result in a surface temperature higher than would have existed on a homogeneous skin. This effect is probably the prime source of difference between theory and experiment. Also, as noted previously, the heat transfer at station 2 is slightly low during the first portion of the flight. If this low value is due to some error in the temperature measurement rather than an actual effect of local flow conditions at station 2, the temperature data for station 8 might give a truer picture of the actual inside wall temperature in the vicinity of stations 2 and 3. As can be seen in figure 15, the agreement between measured and predicted temperature differential is somewhat improved if the data for station 8 are used in place of the data for station 2.

Both experimental and theoretical Stanton numbers are negligibly in error even though this gradient through the skin was not accounted for in the calculations since the gradient has small effect on the slopes $dT_w/d\tau$ and, even at the highest of heating rates, the small temperature differential makes the inside (measured) wall temperature not much different from mean temperature.

Temperature Gradients Over Surface

As would be expected, severe gradients over the surface of the wing were found to exist under the transient aerodynamic heating conditions of this test. Presented in figure 16 is the chordwise temperature distribution at the 42-percent-span station for four different times and Mach numbers during the coasting portion of the flight. (The lines connecting the data points are not fairings, since there were too few measurements to define adequately the distribution, but are merely for identification purposes.)

The changing character of the gradients with time (and therefore heating rate) are clearly indicated. These gradients might be expected to have some influence on the measured data; however, no influence is apparent from comparison of the experimental heat-transfer data with the theory (which is for isothermal surface conditions).

CONCLUSIONS

Rocket-model tests of a wing of aspect ratio 2.9 having a 30° swept leading edge and an unswept trailing edge and employing a hexagonal airfoil section have been made to a Mach number of 3.64 and a Reynolds number of 31.9×10^6 (based on wing mean aerodynamic chord). The data indicate the following results:

1. The highest temperatures and heat-transfer rates occurred at the stagnation line on the leading edge of the wing; however, the temperature measurement technique was inadequate for correlating the data with theory.

2. The Stanton numbers reduced from the temperature time histories for stations other than the stagnation point were in fair agreement with the theoretical results of Van Driest for flat plates with turbulent boundary layers.

3. For the conditions of this test, skin temperatures were predicted with good engineering accuracy by use of Van Driest's theory.

Langley Aeronautical Laboratory,
National Advisory Committee for Aeronautics,
Langley Field, Va., May 29, 1956.

REFERENCES

1. Chauvin, Leo T.: Aerodynamic Heating of Aircraft Components. NACA RM L55L19b, 1956.

2. Carter, Howard S.: Heat Transfer on the Lifting Surfaces of a 60° Delta Wing at Angle of Attack for Mach Number 1.98. NACA RM L56C23, 1956.

3. Sterbutzel, Gerald A., and Kajencki, Stephen S.: Experimental Investigation of Heat Transfer From Aerodynamic Bodies in Supersonic Flow. Rep. No. AF-473-A-9 (Contract W33-038-ac-16701), Cornell Aero. Lab., Inc., Apr. 1950.

4. Rumsey, Charles B., and Lee, Dorothy B.: Measurements of Aerodynamic Heat Transfer and Boundary-Layer Transition on a 10° Cone in Free Flight at Supersonic Mach Numbers up to 5.9. NACA RM L56B07, 1956.

5. Piland, Robert O., Collie, Katherine A., and Stoney, William E.: Turbulent and Laminar Heat-Transfer Measurements on a 1/6-Scale NACA RM-10 Missile in Free Flight to a Mach Number of 4.2 and to a Wall Temperature of 1400° R. NACA RM L56C05, 1956.

6. Ferri, Antonio: Elements of Aerodynamics of Supersonic Flows. The Macmillian Co., 1949.

7. Kelley, K. K.: Contributions to the Data on Theoretical Metallurgy. II. High-Temperature Specific-Heat Equations for Inorganic Substances. Bulletin 371, Bur. Mines, 1934, p. 32.

8. Van Driest, E. R.: The Turbulent Boundary Layer for Compressible Fluids on a Flat Plate With Heat Transfer. Rep. No. AL-997, North American Aviation, Inc., Jan 27, 1950.

9. Van Driest, E. R.: The Turbulent Boundary Layer With Variable Prandtl Number. Rep. No. AL-1914, North American Aviation, Inc., Apr. 2, 1954.

10. Rubesin, Morris W.: A Modified Reynolds Analogy for the Compressible Turbulent Boundary Layer on a Flat Plate. NACA TN 2917, 1953.

11. Beckwith, Ivan E.: Theoretical Investigation of Laminar Heat Transfer on Yawed Cylinders in Supersonic Flow and a Comparison With Experimental Data. NACA RM L55F09, 1955.

12. Churchill, Ruel V.: Modern Operational Mathematics in Engineering. McGraw-Hill Book Co., Inc., 1954, p. 106, problem 7.

13. Coulbert, C. D., MacInnes, W. F., Ishimoto, T., Bussell, B., and Ambrosio, A.: Temperature Response of Infinite Flat-Plates and Slabs to Heat Inputs of Short Duration at One Surface. Contract No. AF33(038)-14381, Univ. of California, Dept. Eng., Apr. 1951.

TABLE I.- WING GEOMETRY

Aspect ratio (based on exposed area in one plane)	2.9
Taper ratio	0.41
Thickness ratio (tip), percent	5.0
Thickness ratio (root), percent	6.4
Leading-edge sweep, deg	30
Trailing-edge sweep, deg	0
Leading-edge wedge angle, deg	4.3
Trailing-edge wedge angle, deg	5.6
Airfoil section	Hexagonal
Mean aerodynamic chord, ft	1.52

TABLE II.- THERMOCOUPLE LOCATIONS

Thermocouple	Span station, in.	Distance from leading edge, in.	Distance from leading edge, percent c
1	14.5	2.38	14.3
2	14.5	7.19	43.7
3	14.5	7.57	46.1
4	14.5	14.44	88.0
5	10.5	0	0
6	10.5	1.62	8.8
7	10.5	3.37	18.4
8	10.5	7.75	42.2
9	10.5	11.75	64.0
10	10.5	16.13	88.0
11	2.0	10.03	43.1
12	2.0	14.78	63.3

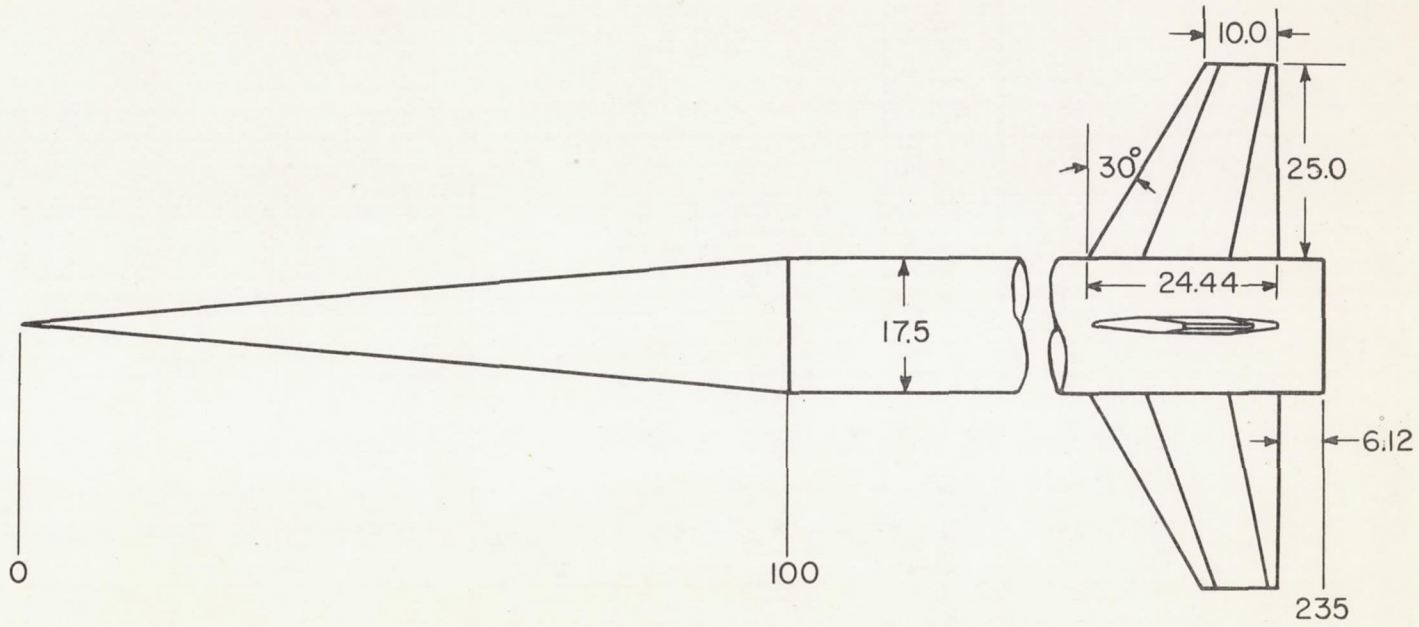

Figure 1.- General arrangement and dimensions of model tested. Dimensions are in inches unless otherwise stated.

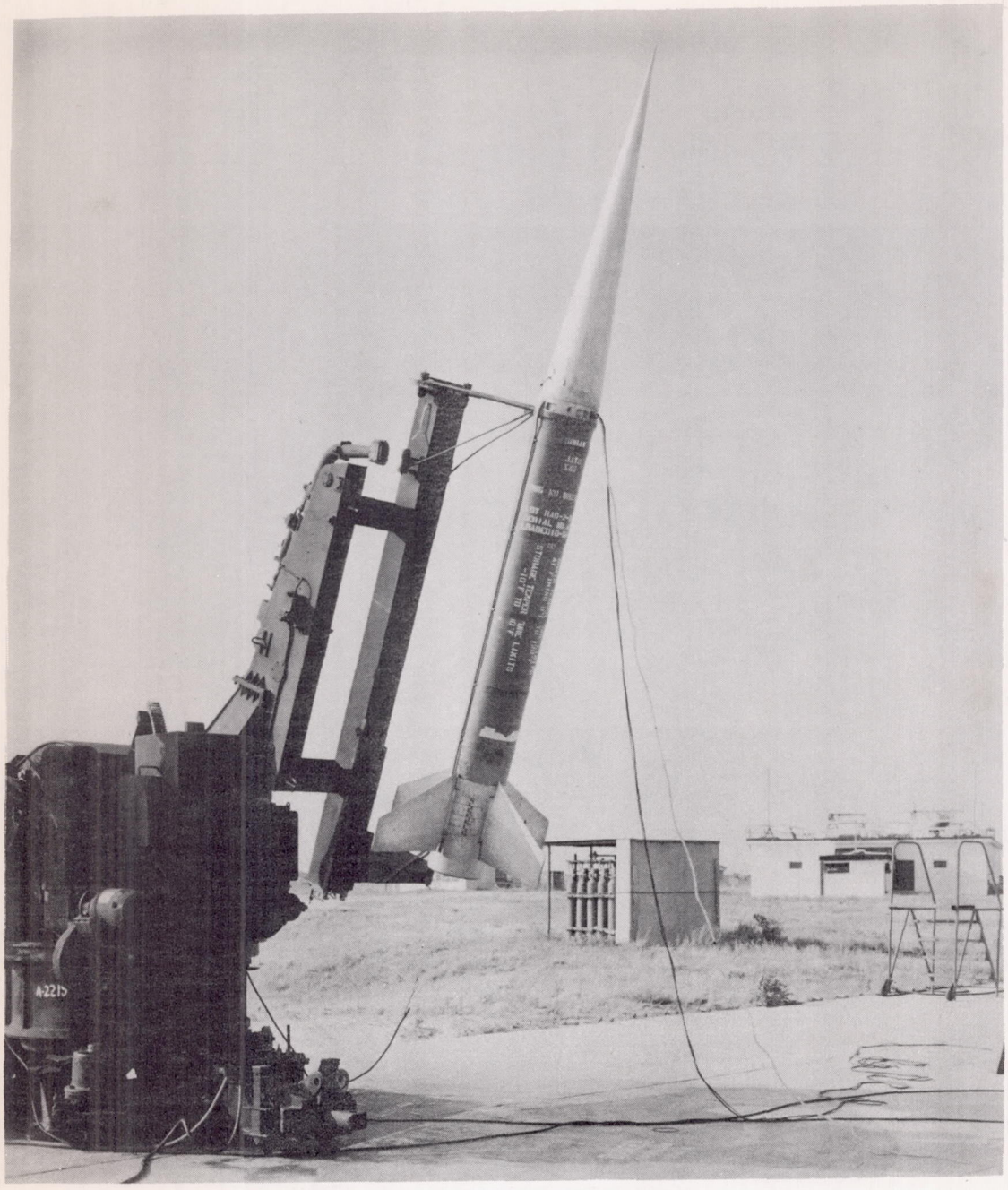

Figure 2.- Rocket model on launcher. L-89648.1

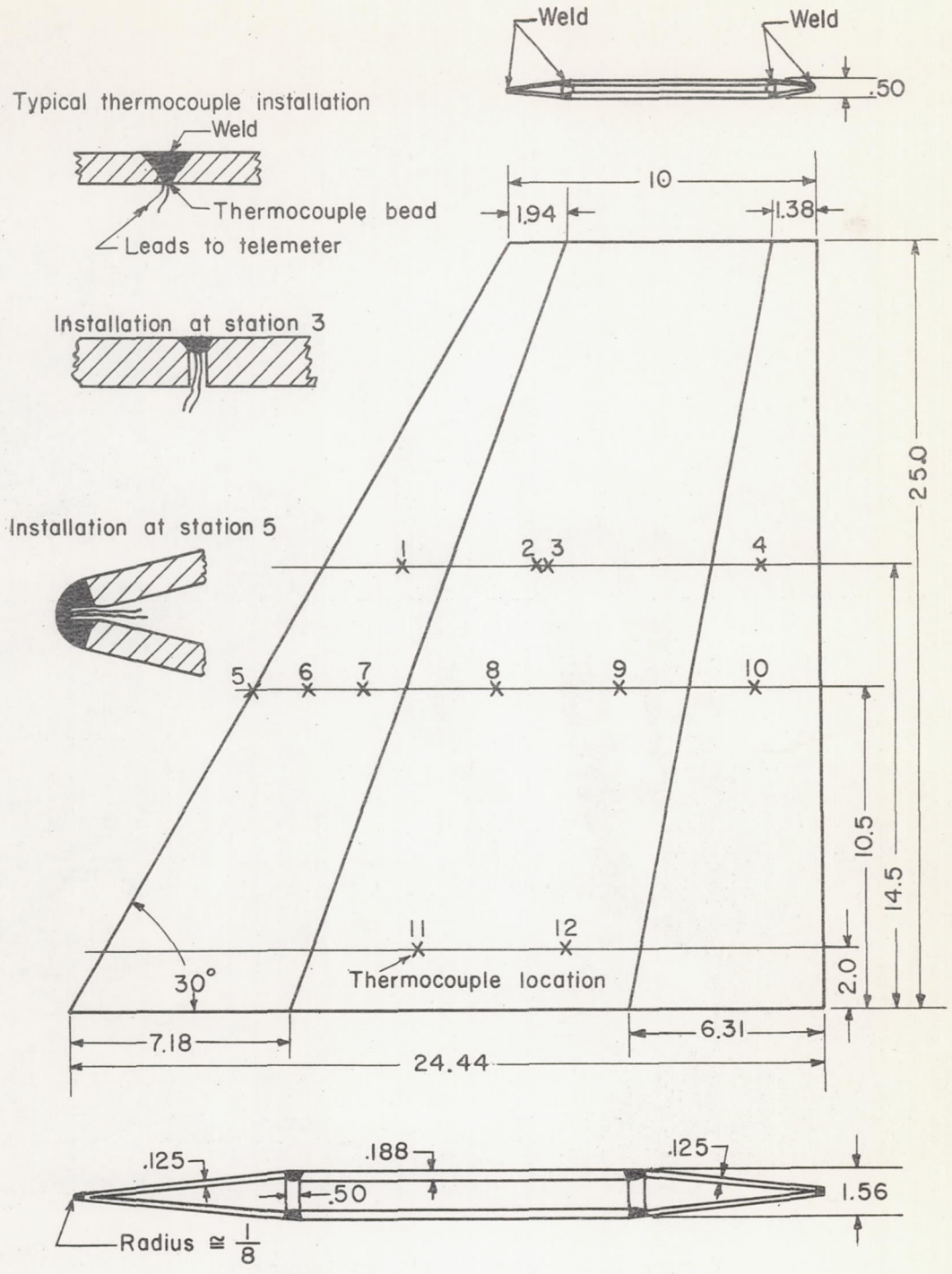

Figure 3.- General arrangement of wing alone. Dimensions are in inches unless otherwise stated.

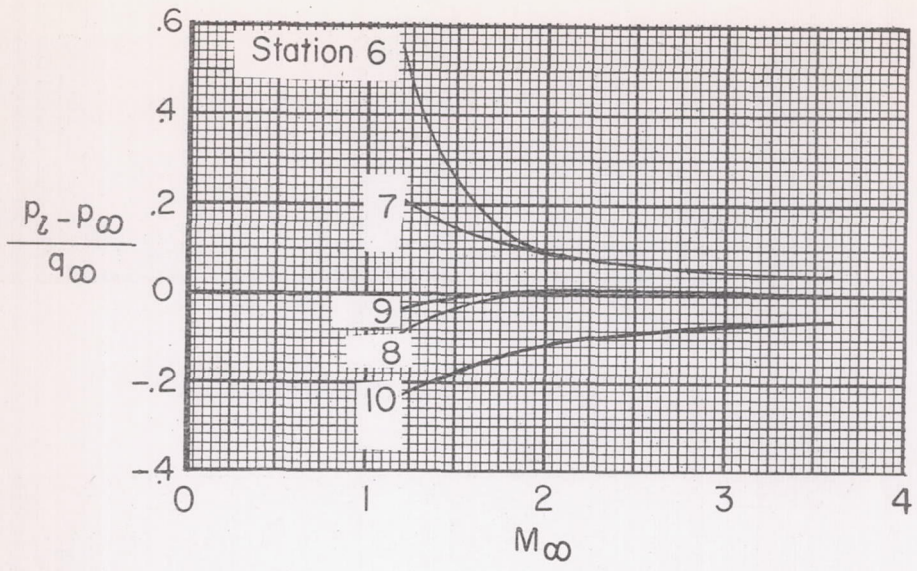

(a) Static-pressure coefficient (from linear theory).

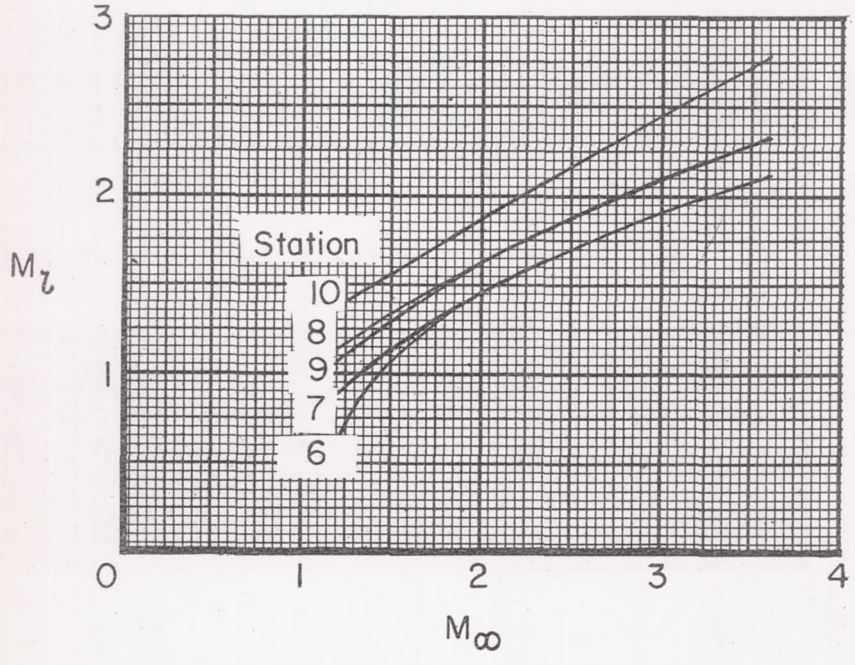

(b) Local Mach number (normal shock at leading edge).

Figure 4.- Local flow parameters as functions of free-stream Mach number.

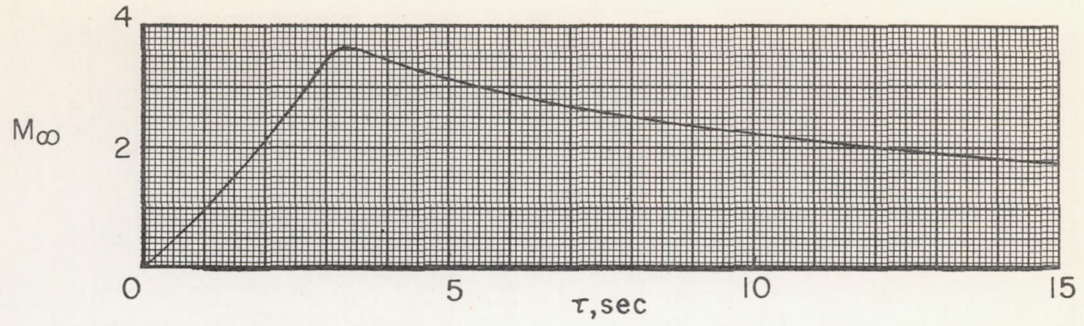

(a) Free-stream Mach number.

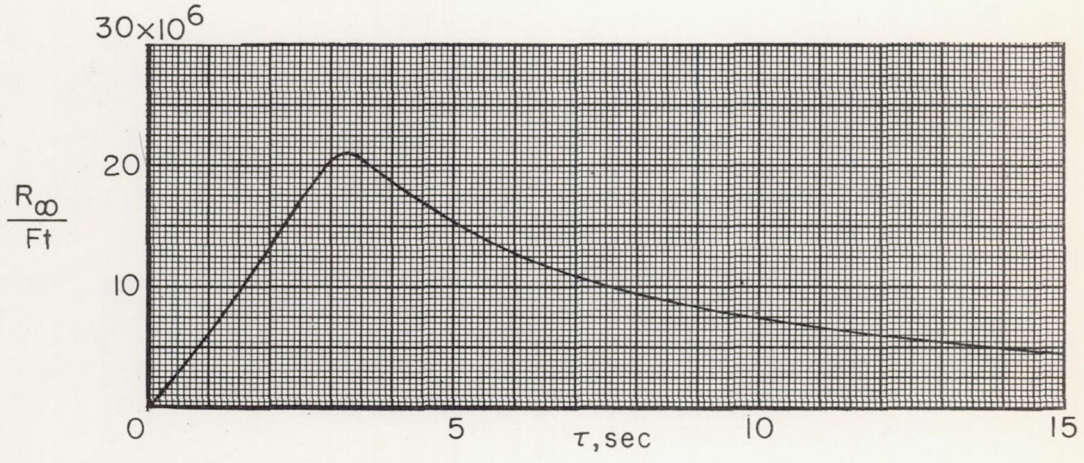

(b) Free-stream Reynolds number per foot.

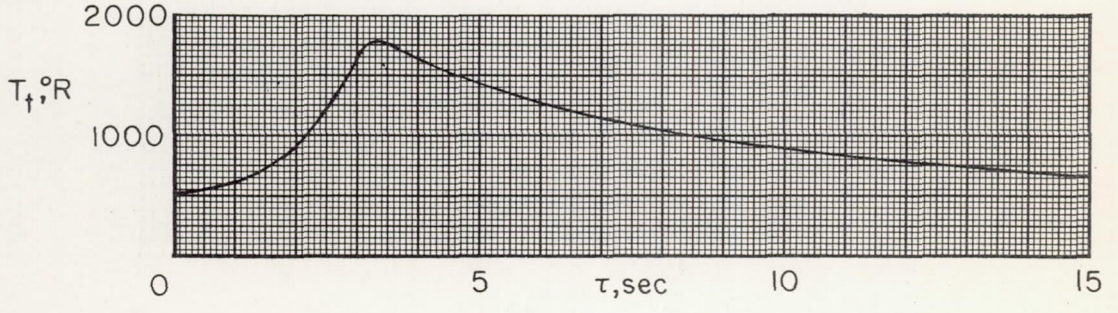

(c) Stagnation temperature.

Figure 5.- Mach number, Reynolds number, and stagnation-temperature time histories.

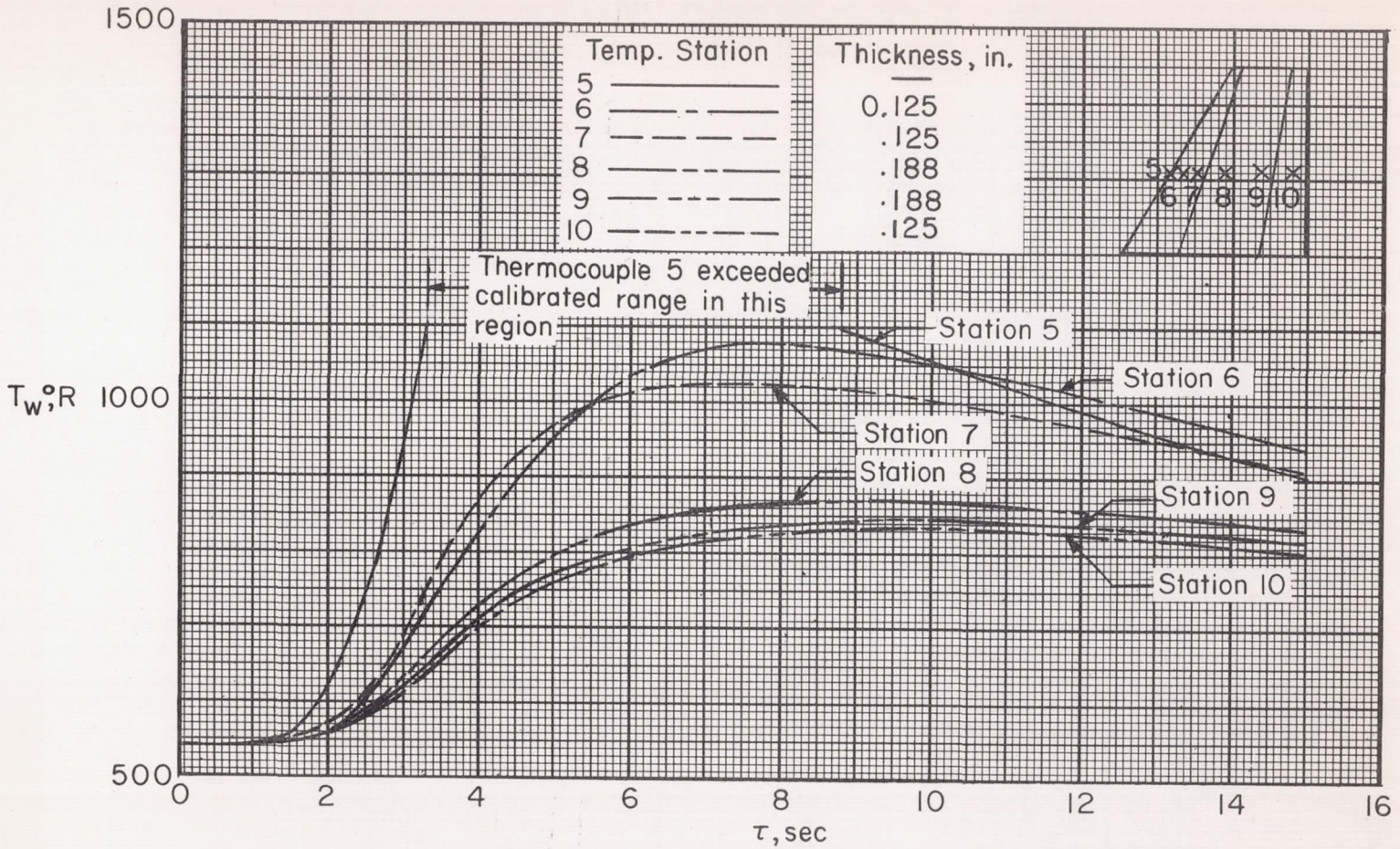

Figure 6.- Temperature time histories. Spanwise station 10.5 (42-percent-span station).

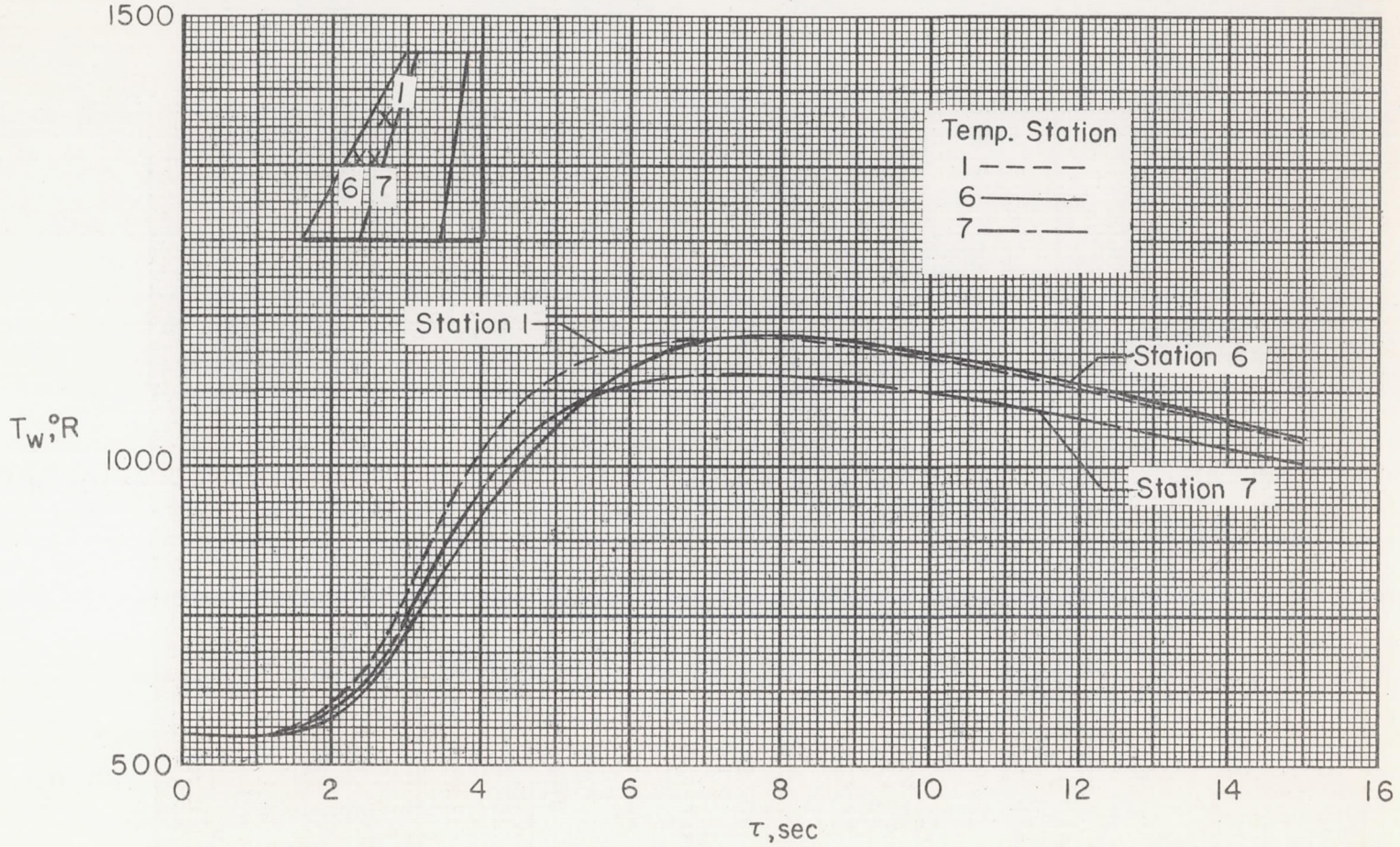

Figure 7.- Temperature time histories. Stations on leading-edge wedge.

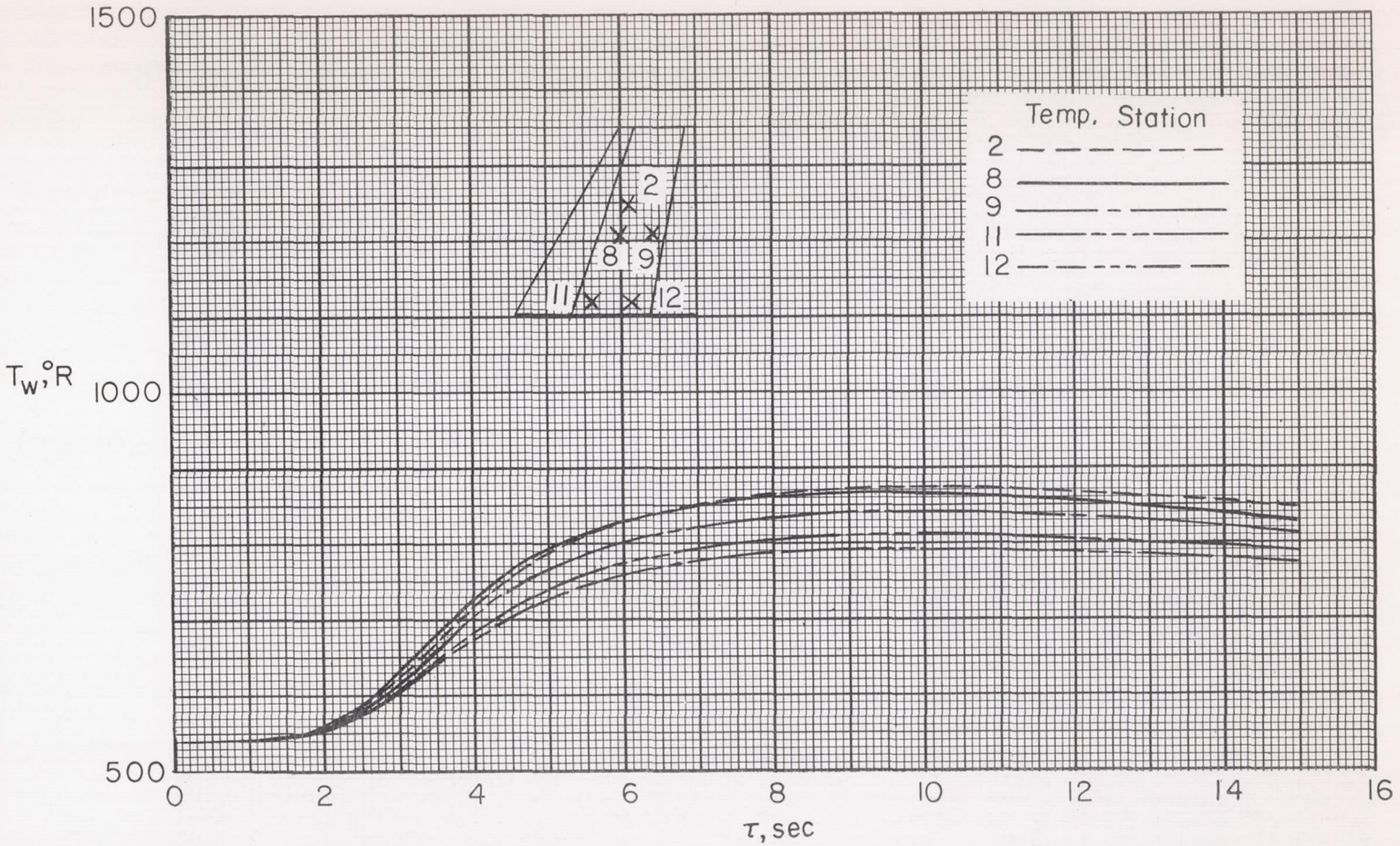

Figure 8.- Temperature time histories. Stations on flat section.

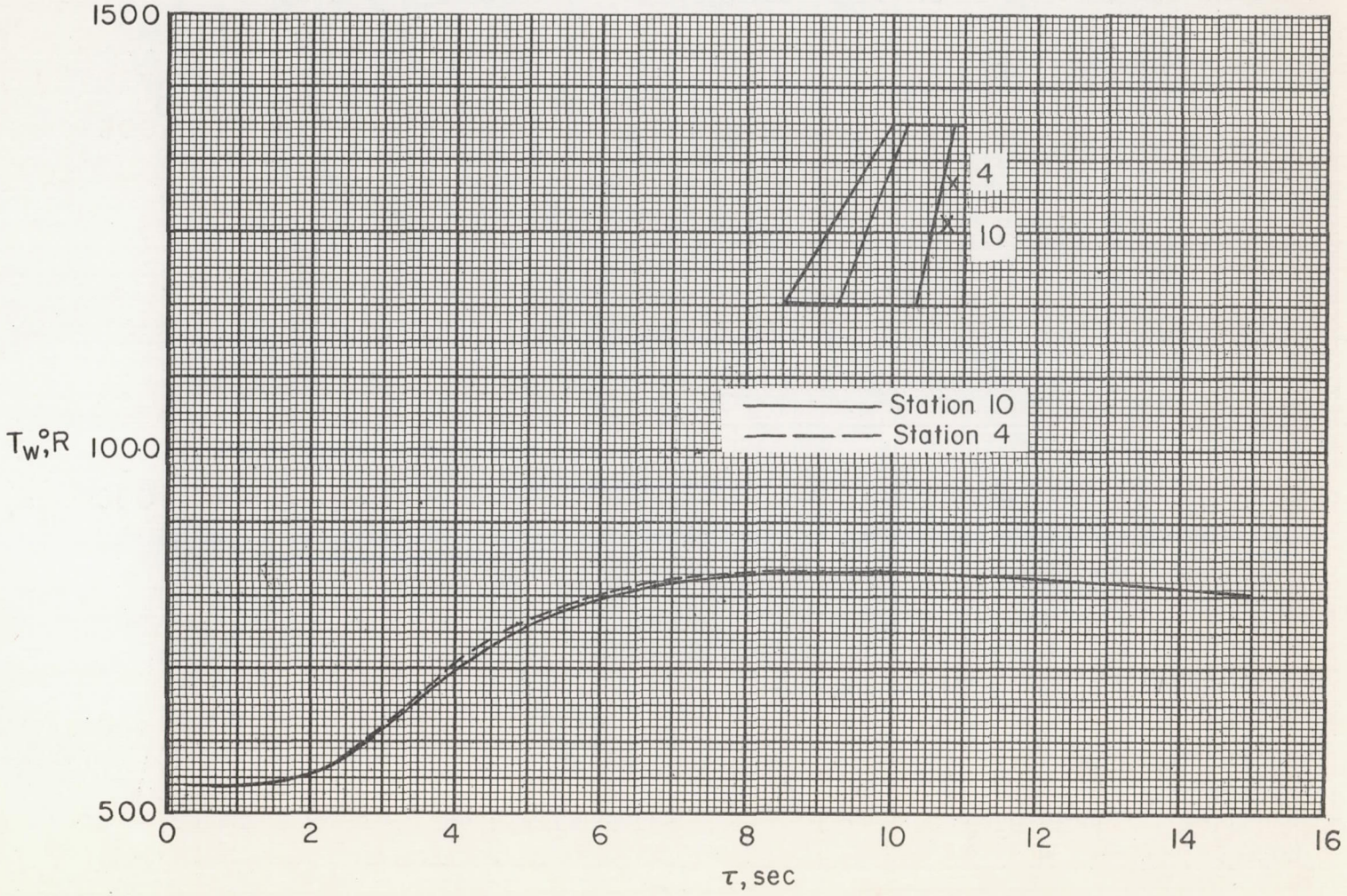

Figure 9.- Temperature time histories. Stations on trailing-edge wedge.

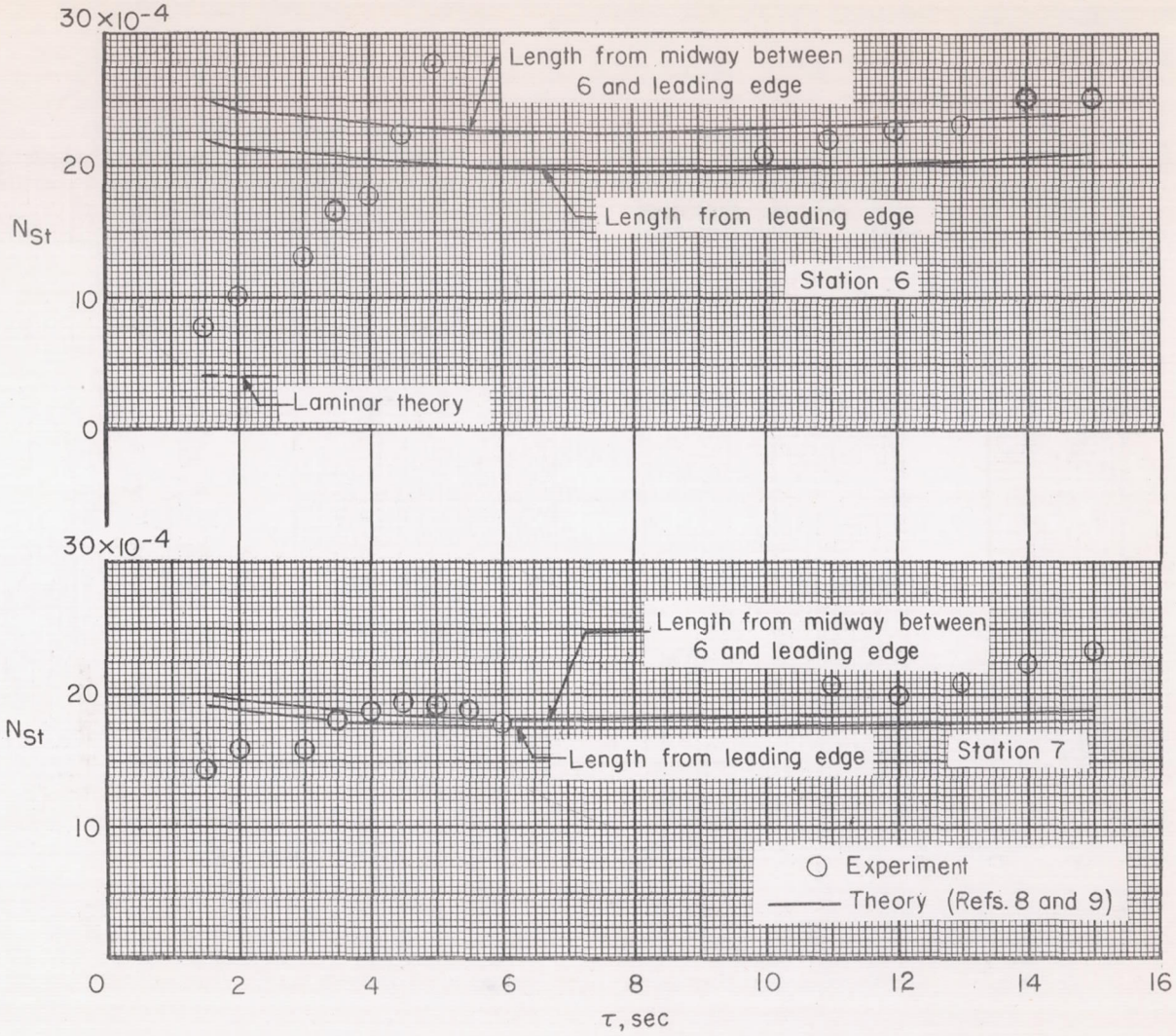

Figure 10.- Stanton number time histories. Stations on leading-edge wedge.

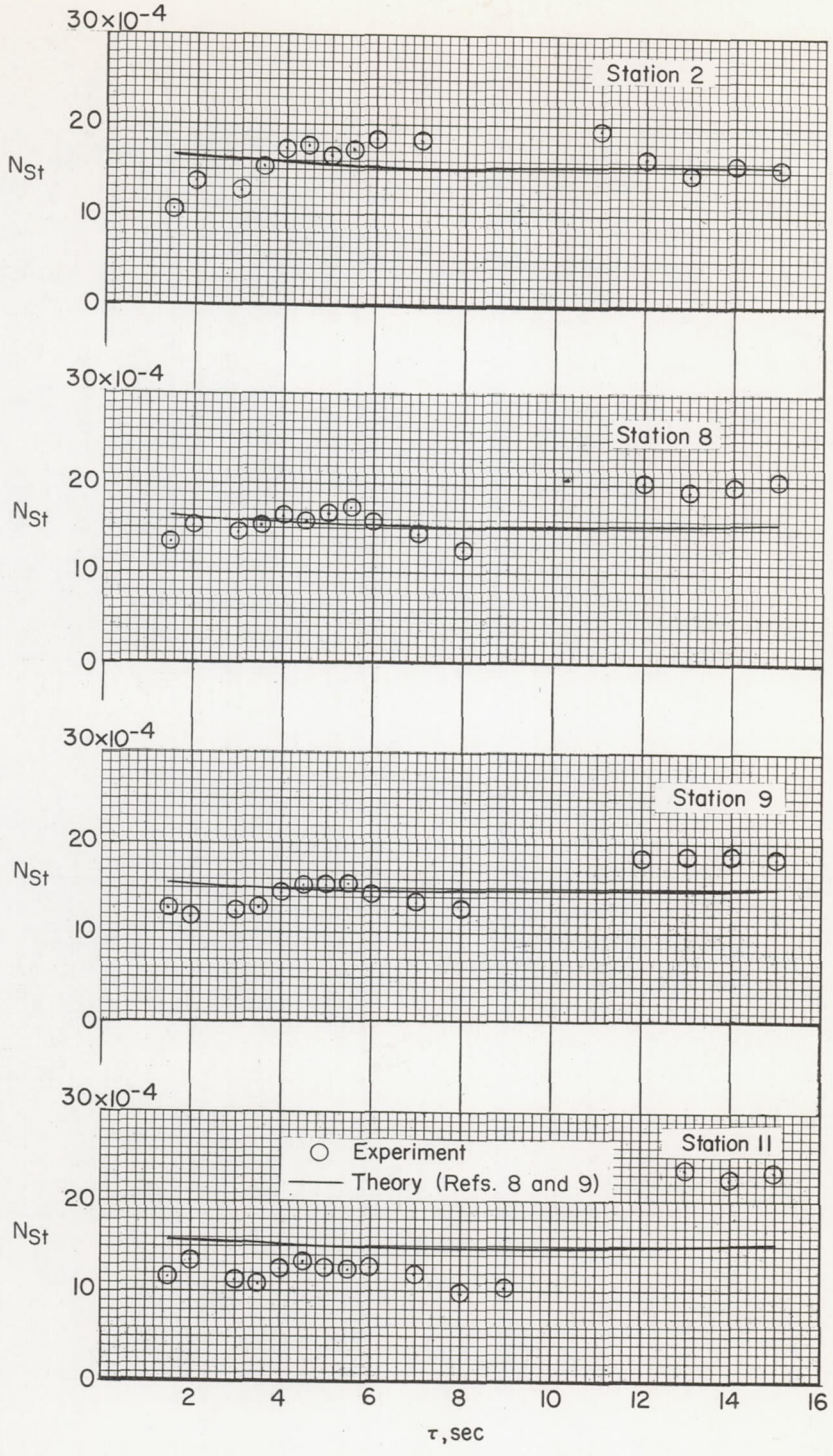

Figure 11.- Stanton number time histories. Stations on flat section.

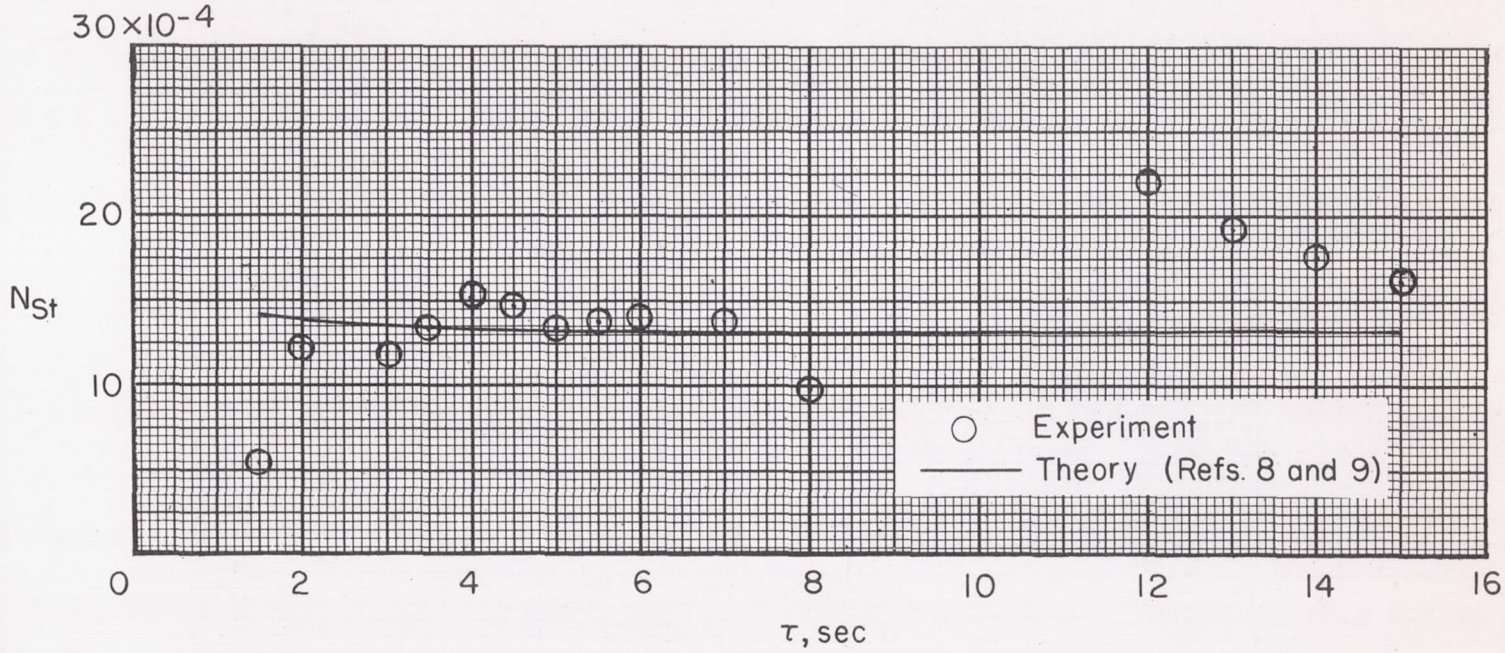

Figure 12.- Stanton number time history. Station 10 on trailing-edge wedge.

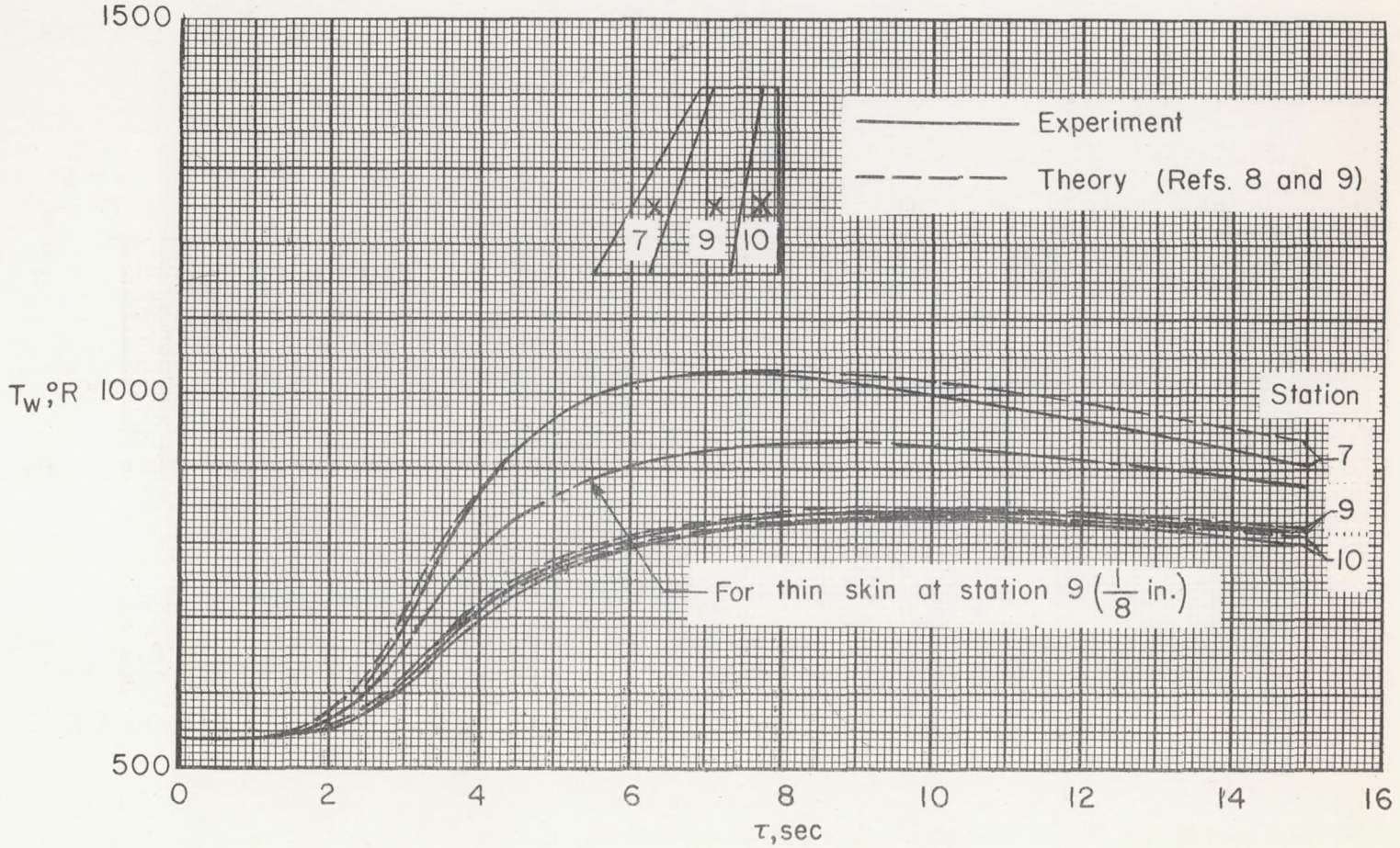

Figure 13.- Comparison of theoretical and experimental temperature time histories.

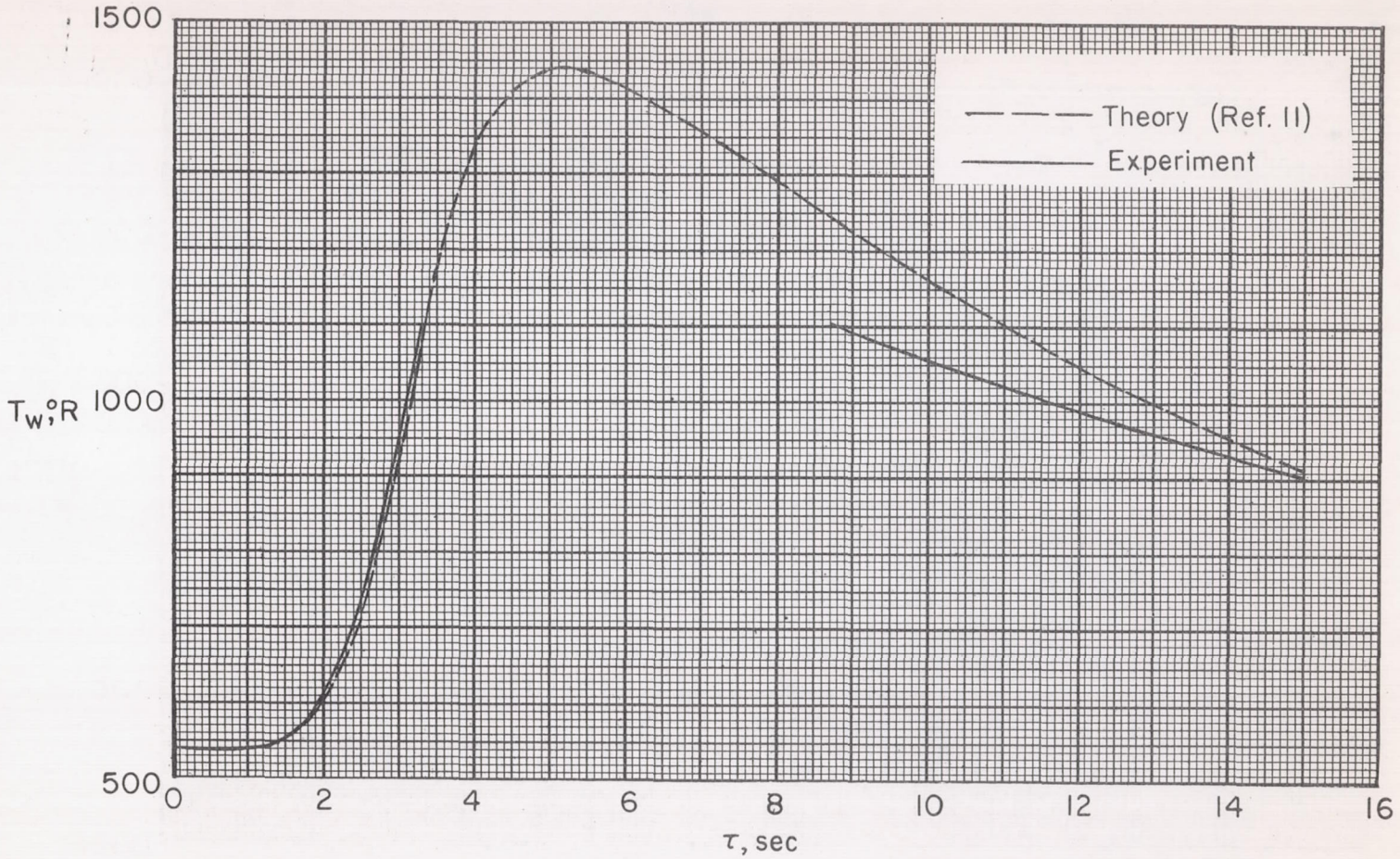

Figure 14.- Temperature at leading-edge stagnation line (station 5).

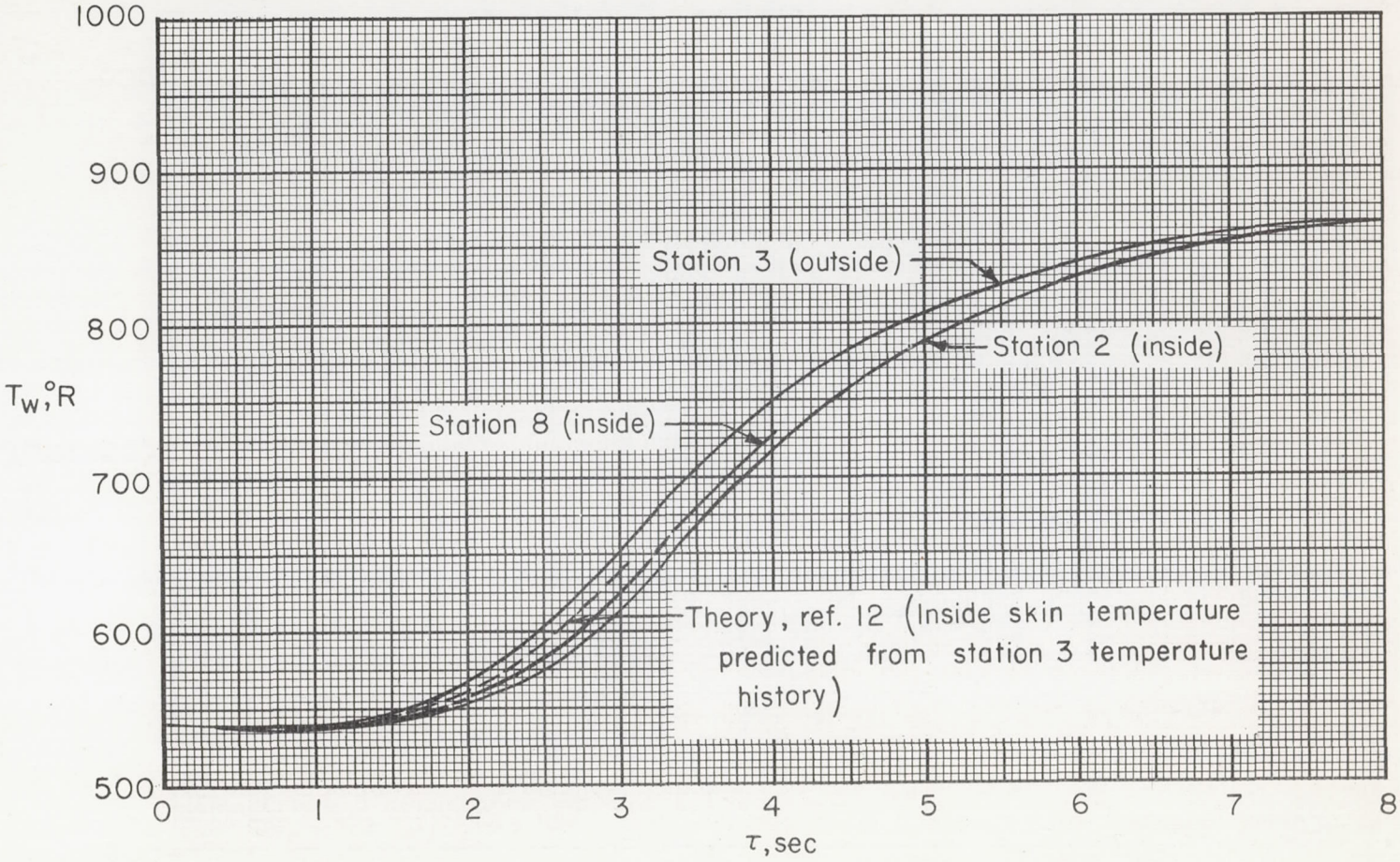

Figure 15.- Comparison of inside and outside skin temperatures.

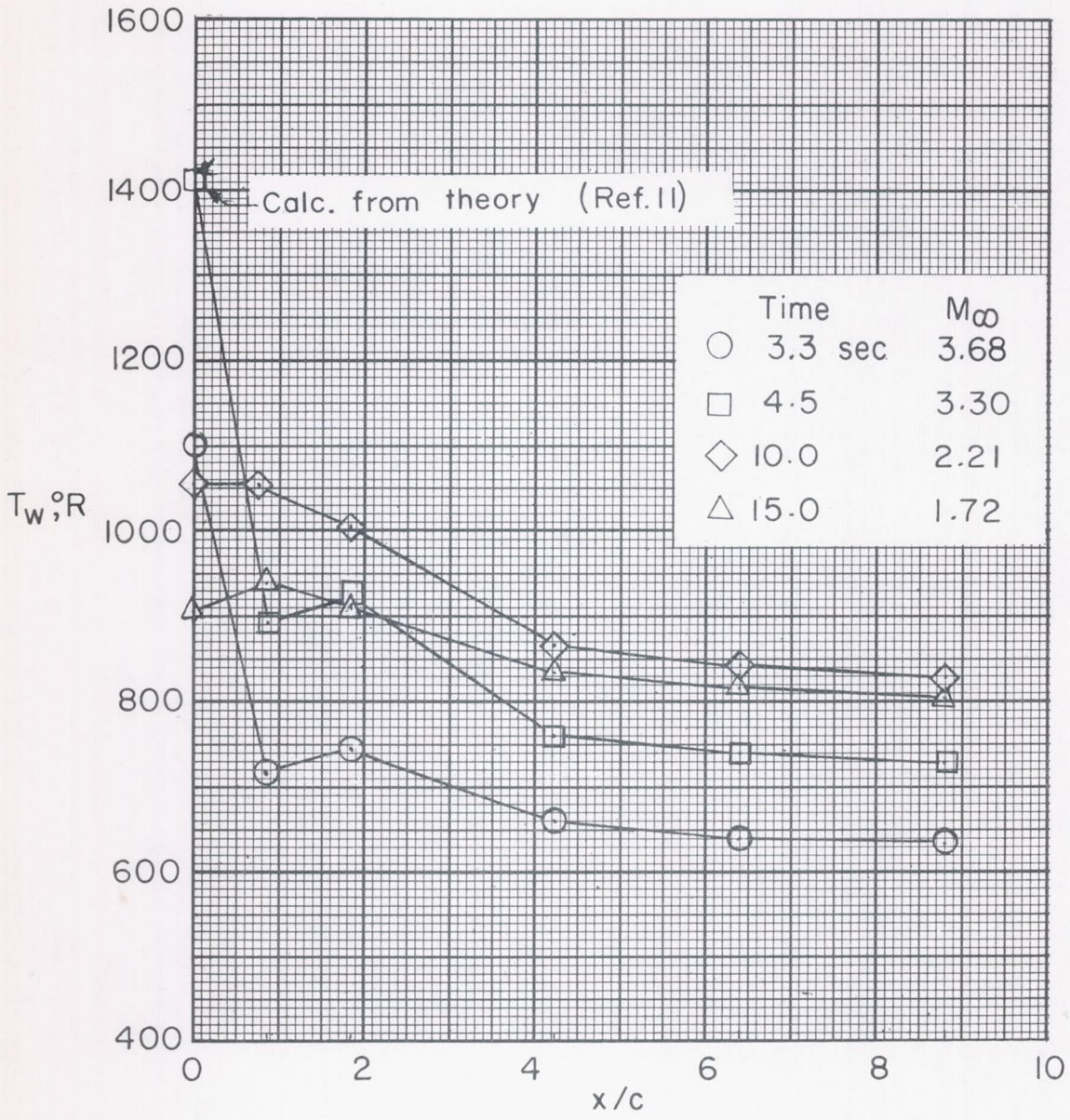

Figure 16.- Chordwise temperature distributions. Spanwise station 10.5 (42-percent-span station).